(Received 17 January 2026, Accepted 13 February 2026, Scheduled 28 February 2026)

Simple Dual-Band Polarization Rotator with Independent Control of Transmissive and Reflective Modes

Ahmed El Yousfi[1, †], Joudi M. Al-Ahmadi[1, †], Abdulrahman M. Alnour Ahmed[2], and Ahmed A. Omar[1, 2, *]

[1] *Interdisciplinary Research Center for Communication Systems and Sensing King Fahd University of Petroleum and Minerals (KFUPM), Dhahran 31261, Saudi Arabia*
[2] *Department of Electrical Engineering, King Fahd University of Petroleum and Minerals (KFUPM) Dhahran 31261, Saudi Arabia*

ABSTRACT: This study proposes an independently controlled polarization rotator with transmissive and reflective capabilities operating in two different frequency bands. The proposed independently controlled transmissive and reflective polarization rotator (ICTR-PR) unit cell consists of four metal layers separated by three substrates. The transmissive polarization rotator mode is realized by two strips (receiving strips) on the top layer, which are connected with two vias through circular holes inside the ground plane to two 90° rotated strips (transmitting strips) on the bottom layer. The reflective polarization rotator mode was produced by connecting another pair of strips on the top layer to a microstrip line located in the middle layer. Properly adjusting the length of each strip allows both transmissive and reflective features to be independently controlled. The proposed rotator exhibits dual-frequency band resonances at 7.7 and 9.48 GHz for reflection and transmission responses, respectively. Furthermore, a high polarization conversion ratio (PCR) of more than 80% was achieved for both modes. A prototype was fabricated and measured to validate the simulation results. A good agreement between the experimental and simulated results was obtained.

1. INTRODUCTION

Polarization rotators have gained increased interest owing to their wide application range, including radar cross section reduction [1] and the development of circularly polarized antennas [2]. Polarization rotators can be classified into reflective [3–6] and transmissive [7–12] types. These structures can rotate the polarization state of the incident electromagnetic wave into its perpendicular counterpart. Most of the work on polarization rotators has been devoted to designing either transmissive or reflective structures. For instance, in [7], a unit cell rotator was proposed for the transmissive mode. The proposed unit cell can rotate the electromagnetic wave into a linear polarization (LP) wave at an angle of 2ϕ (ϕ is the polarization angle) by counterclockwise rotating at 11 GHz. Similarly, another design for the reflective mode was proposed in [4]. It consists of a single-layer unit cell without vias, which rotates the LP waves to its orthogonal counterpart with a polarization conversion ratio PCR of almost 89% and a wideband of 111.5%. Previous designs operated in a single frequency band, thus limiting their application range. To overcome these limitations, several attempts have been made to design rotators with multiband functionalities [13–16]. A triple-band reflective polarization rotator with a high PCR of $\geq$ 90% across the operating bands was presented in [13]. A thin reflective polarization rotator with a dual-band performance was proposed in [15]. Although these designs perform well in terms of PCR and bandwidth, their main drawback lies in their ability to work only in one mode, either transmissive or reflective, which may limit their range of applications.

To meet the current demand for wireless devices, it is challenging to integrate more functionalities into one unit cell, such as transmissive and reflective functionalities, while maintaining good performance. Achieving this can significantly reduce the bulk and complexity of radio frequency (RF) devices. In [17], a metamaterial unit cell rotator based on a split-ring resonator was proposed to rotate transmitted and reflected electromagnetic waves simultaneously. The structure presented up to 95% PCR in the transmissive mode at the lower band, whereas in the reflective mode, a PCR of 93% was achieved in the higher band under normal incidence. Another technique based on the exploitation of the phase transition of vanadium dioxide (VO_2), a metamaterial unit cell with both reflective and transmissive polarization conversions, was presented in the THz domain [18]. When the VO_2 is a metal, the design acts as a reflective cross-polarization rotator. However, when VO_2 is an insulator, the structure behaves as a transmissive cross-polarization rotator with a PCR of 90% over the operating bands. However, phase transition control requires external intervention to change the phase (electric field, temperature, etc.), which makes the design complex. Recently, a single-layer S-shaped metasurface was presented to obtain simultaneous reflective and transmissive polarization rotations [19]. However, the PCR values in the transmissive and reflective polarization modes were 60%

* Corresponding author: Ahmed Abdelmottaleb Omar (ahmed.omar.1@kfup-m.edu.sa).
† Authors contributed equally to this work.

and 70%, respectively. Other researchers have integrated PIN diodes in metasurfaces to achieve reconfigurability with multiple functions [20, 21]. However, implementing many diodes (at least one per unit cell) will increase the complexity of the design. To the best of our knowledge, no transmissive and reflective polarization rotators (TRPRs) with independent frequency control and simple design methodology have been proposed in the literature.

This article proposes a simple unit cell design, an independent controlled transmissive and reflective polarization rotator ICTR-PR, using a pair of strips connected through vias. Independent frequency control can be easily achieved by properly adjusting the strip length. Section 2 introduces the proposed design with a performance analysis to demonstrate the independent frequency control. The proposed design is fabricated and measured in Section 3. Finally, conclusions are presented in Section 4.

2. PROPOSED TRANSMISSIVE AND REFLECTIVE POLARIZATION ROTATOR

2.1. Proposed Unit Cell

The proposed ICTR-PR unit cell is shown in Fig. 1. The unit cell size was $20 \times 20\,\text{mm}^2$ ($0.5 \times 0.5\lambda_0^2$ where λ_0 is the free space wavelength at 7.7 GHz). It is composed of four metallic layers labeled M_1, M_2, M_3, and M_4 separated by three substrates. The top metallic layer, M_1, contains two pairs of orthogonal rectangular strips printed on an F4-B substrate with a relative permittivity of 2.6, loss tangent of 0.002, and thickness $h_1 = 3.2\,\text{mm}$. The pair of strips at the top-left corner (receiving strips) is connected to those located in the bottom layer (transmitting strips), M_4, through metallic vias to enable transmissive polarization rotation. The bottom metal plane, M_4, is printed on the same substrate with a thickness $h_3 = 1.7\,\text{mm}$. The middle metallic layers, M_2 and M_3, are the ground plane and microstrip line, respectively, and are printed on the same substrate with thickness $h_2 = 1.6\,\text{mm}$. The top orthogonal strips in the bottom-right corner of M_1 are connected by two coaxial vias with a microstrip line in M_3 for reflective polarization rotation.

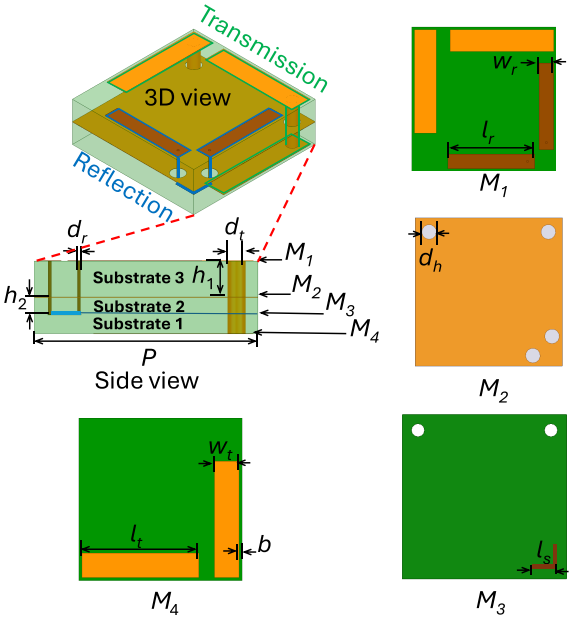

FIGURE 1. Geometry of the proposed ICTR-PR unit cell. The geometric dimensions are $P = 20$, $l_t = 14.3$, $l_r = 12$, $w_t = 3$, $w_r = 2$, $h_1 = 3.2$, $h_2 = 1.6$, $b = 0.4$, $d_t = 1.6$, $d_r = 0.3$, $l_s = 3$, $d_h = 2$, $h_3 = 1.7$, $W_s = 0.43$ (unit: mm).

All full-wave simulations were performed using the Ansys High-Frequency Structure Simulator (HFSS). The simulated co-reflection, cross-reflection, and cross-transmission coefficients are shown in Fig. 2(a). As can be seen, the proposed unit cell exhibits a reflective polarization rotation mode at 7.7 GHz, whereas at 9.48 GHz it allows a transmissive polarization rotation mode. It is worth noting that the proposed design exhibits an insertion loss of 0.9 dB and 0.86 dB at 7.75 GHz and 9.36 GHz for the reflective mode and the transmissive modes, respectively. Moreover, the proposed design achieves a suppression level of 28.8 dB and 10.62 dB at 7.75 GHz and 9.36 GHz in the reflective and transmissive modes, respectively.

The polarization conversion ratio (PCR) was calculated for both transmissive and reflective modes using the following equation:

$$\text{PCR}_{t,r} = \frac{|S_{ijxy}|^2}{|S_{ijxy}|^2 + |S_{ijxx}|^2}; \quad i,j = 1,2 \tag{1}$$

where t and r are the transmission and reflection modes, respectively. Note that when $i = j$, the mode is reflective, whereas when $i \neq j$, the mode is transmissive. Fig. 2(b) shows that the proposed unit cell exhibits a PCR of more than 80% over the frequency band of 2.6% (7.67–7.87 GHz) and 3.1% (9.25–9.54 GHz) in reflective and transmissive modes, respectively. This narrowband behavior is attributed to the fact that the proposed rotator exhibits only a single resonant frequency. This is mainly due to employing strip resonators for each band. One way to increase the bandwidth (BW) is to use another strip resonator with a different length to create another resonant frequency. This may be a topic for future work.

2.2. Performance Analysis

This section demonstrates the ability of the proposed ICTR-PR unit cell to operate independently in the transmission and reflection polarization modes. To validate this, a parametric study of key design parameters was conducted and shown in Fig. 3. Fig. 3(a) presents the impact of varying the strip length, "l_r", on the co-reflection, cross-reflection coefficients, and co-transmission coefficient. As "l_r" increases, the resonance frequency of the reflective polarization rotator shifts downward to 7.5 GHz, whereas the cross-transmission coefficient at the higher frequency remains unaffected. This behavior confirms the ability of the unit cell to independently control the operating frequency in the reflection mode. Similarly, in the higher-frequency band, increasing the length of the transmitting strip, "l_t", results in a decrease in the resonance frequency, with no noticeable effect on the lower-frequency band, as illustrated in Fig. 3(b). This further supports the independent tunability of the unit cell in transmission and reflection modes. The simulated vector surface current distribution at 7.7 and 9.48 GHz is

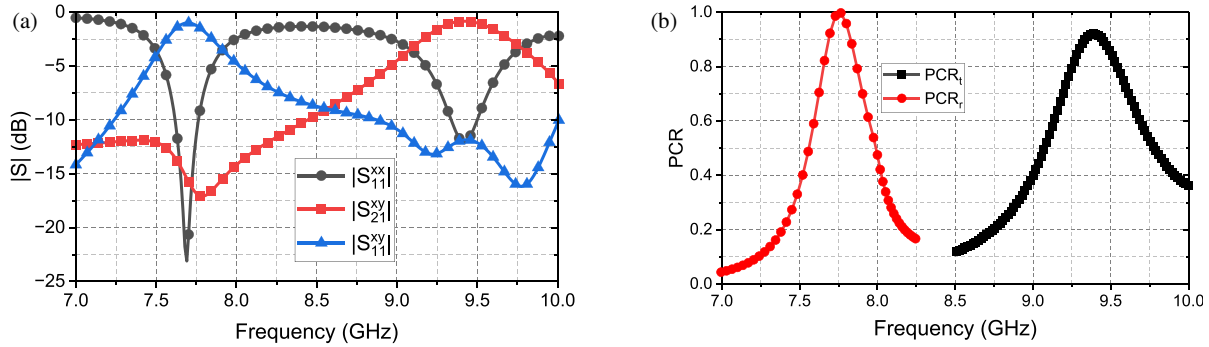

FIGURE 2. (a) Simulated S-parameters of the proposed unit cell design. (b) Simulated polarization conversion ratio (PCR) of transmission and reflection modes.

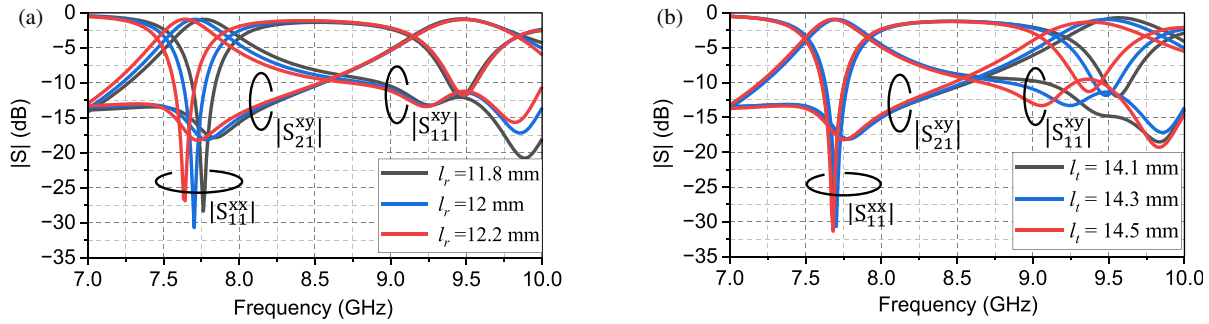

FIGURE 3. (a) Effect of the reflective strip length on S-parameters of the proposed unit cell. (b) Effect of the transmissive strip length on the S-parameters of the proposed unit cell.

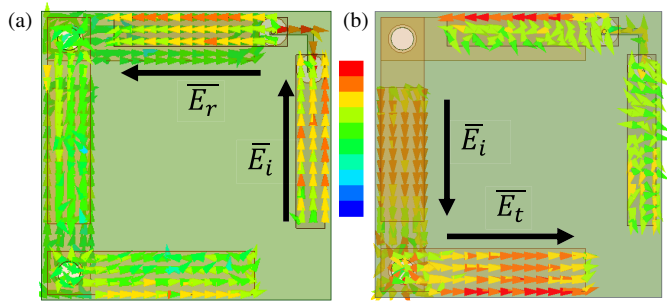

FIGURE 4. Simulated vector surface current distribution of the proposed unit cell at (a) 7.7 and (b) 9.48 GHz.

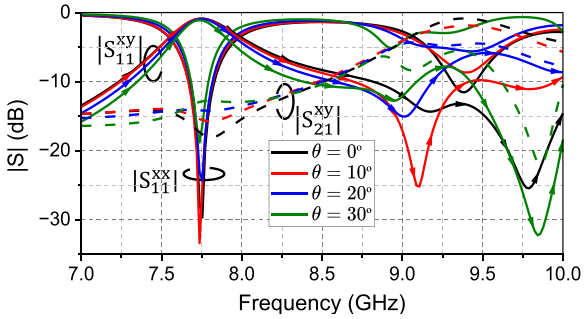

FIGURE 5. Simulated S-parameters of the proposed unit cell design under oblique incidence for TE mode.

illustrated in Fig. 4. The black arrows indicate the manner in which the incident electric field $\overline{E_i}$ is rotated in both modes. It is seen that at 7.7 GHz (Fig. 4(a)), most of the current is uniformly concentrated around the two strips used for the reflection polarization rotator (top right corner). In contrast, at 9.48 GHz, the current is uniformly distributed along the strips responsible for the transmission mode (bottom left corner). This indicates that the proposed ICTR-PR unit cell can be independently controlled in the transmissive and reflective modes.

Finally, to investigate the angular stability of the proposed unit-cell design under oblique incidence, the variation of the incident angle θ for the TE mode is presented in Fig. 5. As shown, for the reflective mode, the proposed rotator is almost insensitive to the oblique incidence angle. However, the performance of the transmissive mode is considered sensitive under oblique incidence. It is important to note that, for the TM mode, the results are similar and are omitted for brevity.

3. FABRICATION AND MEASUREMENT

To validate the simulation results, the proposed ICTR-PR unit cell design was fabricated and experimentally measured. A photograph of the fabricated prototype is shown in Fig. 6(a). The fabricated structure measured approximately $30 \times 30\,\text{cm}^2$, comprising 15×15 unit cells. In the fabrication process, three F4-B substrate layers with a relative permittivity of 2.6 are employed, on which the conducting strips are printed. The first two layers, containing the reflective part, are stacked together by the company, while the transmissive part was printed separately and later stacked employing copper via holes for connect-

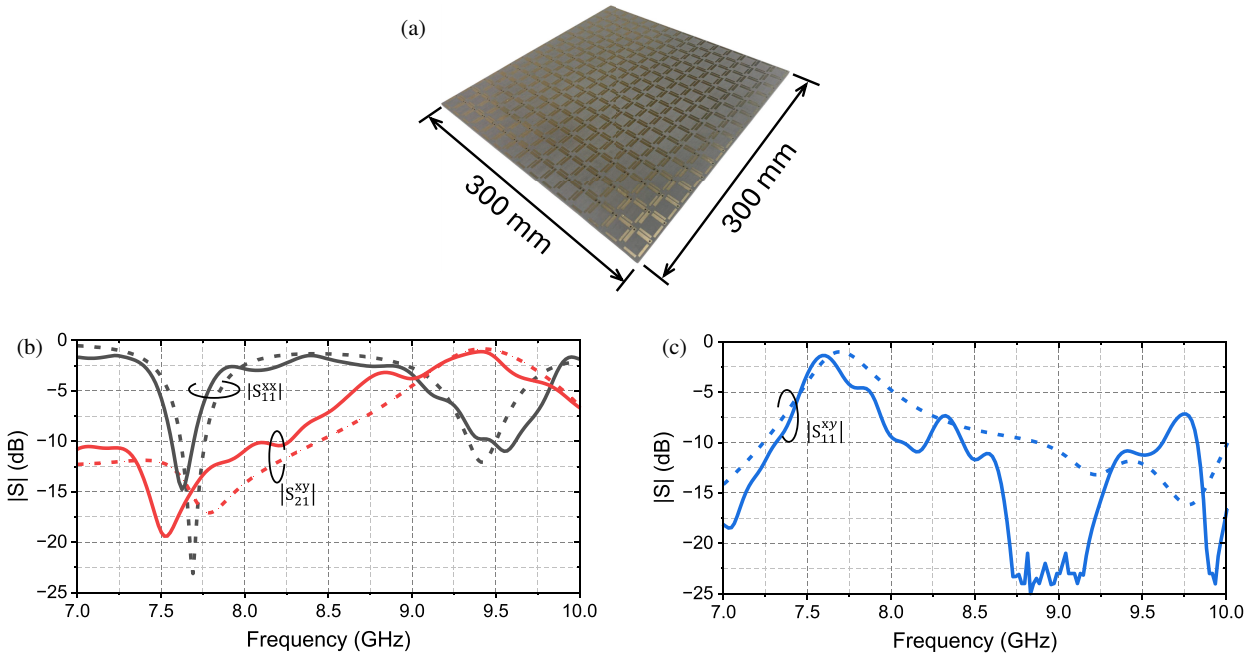

FIGURE 6. (a) Photograph of the fabricated structure of 15×15. (b) Simulated and measured co and cross polarization reflection and transmission coefficients. (c) Simulated and measured cross-polarization reflection coefficient. (Measured results are presented by solid lines, while simulated ones are shown with dashed lines).

TABLE 1. Performance comparison of the proposed unit cell with recent works.

Ref.	Operating band (GHz)	Unit cell size λ_0^3	Type	PCR (%)	Freq. Control	Oblique incidence	No. Layers	Complexity
[18]	500–4750 4800–13130	–	T R	> 90 > 90	No	$< 40°$	4	Complex (Vanadium injection)
[19]	7.07–7.46 16.6–16.6	$0.26 \times 0.26 \times 0.05$	T R	> 60 > 70	No	NA	2	Simple
[20]	5.8–7.4 5.4–9.4	$0.39 \times 0.39 \times 0.18$	T R	> 90 > 90	No. but reconfigurable	50°	3	Complex (pin diodes + inductor)
[22]	4–7.50 12–20	$0.42 \times 0.42 \times 0.15$	T R	— —	No. but reconfigurable	NA	4	Complex (pin diodes + inductor)
Our work	**7.67–7.87** **9.25–9.54**	$0.49 \times 0.49 \times 0.25$	**R** **T**	> 80 > 80	**Yes**	15° (T) 40° (R)	4	**Simple**

ing the transmissive strips. The vias are subsequently soldered to ensure reliable electrical contact. The thickness tolerance of the dielectric substrates depends on the thickness of each layer and ranges from 0.05 mm for the thinnest substrate to 0.13 mm for the thickest one. Two sets of standard-gain linearly polarized horn antennas connected to a vector network analyzer were used in the measurement setup. A comparison between the simulated and measured results under normal incidence is illustrated in Figs. 6(b) and (c), which shows that the measured data are in good agreement with the simulated results. Minor discrepancies are due to the fabrication and material tolerance, and the misalignment of horn antennas.

Finally, Table 1 compares the proposed design with recent studies to highlight its advantages. Overall, the proposed unit cell can independently control the frequency bands while having a simple and easy geometry (from the design methodology point of view). For instance, [19] has a simple structure with two layers, but at the expense of a low PCR of 60%. On the other hand, [18, 20, 22] show a high PCR with wideband performance and a comparable number of layers; however, using either many diodes or injection techniques might increase the fabrication cost and complexity of the entire structure. It is important to emphasize that, although the proposed design has four metallic layers, its simplicity resides in the design methodology used to achieve transmissive and reflective polarization features, which are obtained without adding external components/elements to control the function of the polarization rotator, as often reported in the existing works, such as using diodes along with biasing circuits or injection methods.

4. CONCLUSION

A simple dual-band polarization rotator with simultaneous transmissive and reflective characteristics in a single unit cell that exhibits good performance was proposed. The proposed design exhibited independent frequency control, with a PCR of more than 80% over the frequency bands of 2.6% (7.67–7.87 GHz) and 3.1% (9.25–9.54 GHz) in the reflective and transmissive modes, respectively. The current distribution and parametric study were used to analyze the working principle of the structure. Finally, the design is fabricated and measured to validate the simulation results.

ACKNOWLEDGEMENT

This work was supported by the Deanship of Research at King Fahd University of Petroleum and Minerals (KFUPM) under the Interdisciplinary Research Center for Communication Systems and Sensing (IRC-CSS) under Project INCS2508.

REFERENCES

[1] Al-Nuaimi, M. K. T., G.-L. Huang, W. G. Whittow, D. Wang, R.-S. Chen, S.-W. Wong, and K.-W. Tam, "Coding engineered reflector for wide-band RCS reduction under wide angle of incidence," *IEEE Transactions on Antennas and Propagation*, Vol. 70, No. 10, 9947–9952, 2022.

[2] Li, W., S. Gao, Y. Cai, Q. Luo, M. Sobhy, G. Wei, J. Xu, J. Li, C. Wu, and Z. Cheng, "Polarization-reconfigurable circularly polarized planar antenna using switchable polarizer," *IEEE Transactions on Antennas and Propagation*, Vol. 65, No. 9, 4470–4477, 2017.

[3] Zhao, Y.-T., J.-J. Zhang, and B. Wu, "Low profile reflective polarization conversion metasurface with high frequency selectivity," *IEEE Transactions on Antennas and Propagation*, Vol. 70, No. 11, 10 614–10 622, 2022.

[4] Omar, A. A., W. Hong, A. Al-Awamry, and A.-E. Mahmoud, "A single-layer vialess wideband reflective polarization rotator utilizing perforated holes," *IEEE Antennas and Wireless Propagation Letters*, Vol. 19, No. 12, 2053–2056, 2020.

[5] Jia, Y., Y. Liu, Y. J. Guo, K. Li, and S.-X. Gong, "Broadband polarization rotation reflective surfaces and their applications to RCS reduction," *IEEE Transactions on Antennas and Propagation*, Vol. 64, No. 1, 179–188, 2016.

[6] Jia, Y., Y. Liu, Y. J. Guo, K. Li, and S. Gong, "A dual-patch polarization rotation reflective surface and its application to ultra-wideband RCS reduction," *IEEE Transactions on Antennas and Propagation*, Vol. 65, No. 6, 3291–3295, 2017.

[7] Ding, G., L. Chen, J. Bi, K. Qu, S. Chen, X. Luo, K. Chen, and S. Wang, "Flexible rotation of linear polarization conversion with a frequency selective surface," *Optics Express*, Vol. 31, No. 25, 41 658–41 668, Dec. 2023.

[8] Wang, S.-Y., J.-D. Bi, W. Liu, W. Geyi, and S. Gao, "Polarization-insensitive cross-polarization converter," *IEEE Transactions on Antennas and Propagation*, Vol. 69, No. 8, 4670–4680, 2021.

[9] Wang, S.-Y., W. Liu, and W. Geyi, "Dual-band transmission polarization converter based on planar-dipole pair frequency selective surface," *Scientific Reports*, Vol. 8, No. 1, 3791, 2018.

[10] Hill, N. and S. Cornbleet, "Microwave transmission through a series of inclined gratings," *Proceedings of the Institution of Electrical Engineers*, Vol. 120, No. 4, 407–412, 1973.

[11] Omar, A. A., Z. Shen, and S. Y. Ho, "Multiband and wideband 90° polarization rotators," *IEEE Antennas and Wireless Propagation Letters*, Vol. 17, No. 10, 1822–1826, 2018.

[12] Omar, A. A., A. Mahmoud, J. Choi, and W. Hong, "Wideband transmissive polarization rotator with in-band notches enabling multiband operation," *IEEE Access*, Vol. 9, 44 751–44 756, 2021.

[13] Babu, B. A., B. T. P. Madhav, S. Das, N. Hussain, S. S. Ali, and N. Kim, "A triple-band reflective polarization conversion metasurface with high polarization conversion ratio for ISM and X-band applications," *Sensors*, Vol. 22, No. 21, 8213, 2022.

[14] Kamal, B., J. Chen, Y. Yin, J. Ren, S. Ullah, and U. Ali, "Design and experimental analysis of dual-band polarization converting metasurface," *IEEE Antennas and Wireless Propagation Letters*, Vol. 20, No. 8, 1409–1413, 2021.

[15] Khan, B., B. Kamal, S. Ullah, I. Khan, J. A. Shah, and J. Chen, "Design and experimental analysis of dual-band polarization converting metasurface for microwave applications," *Scientific Reports*, Vol. 10, No. 1, 15393, 2020.

[16] Fu, C., Z. Sun, L. Han, C. Liu, T. Sun, and P. K. Chu, "High-efficiency dual-frequency reflective linear polarization converter based on metasurface for microwave bands," *Applied Sciences*, Vol. 9, No. 9, 1910, 2019.

[17] Li, F., H. Chen, Q. He, Y. Zhou, L. Zhang, X. Weng, H. Lu, J. Xie, and L. Deng, "Design and implementation of metamaterial polarization converter with the reflection and transmission polarization conversion simultaneously," *Journal of Optics*, Vol. 21, No. 4, 045102, 2019.

[18] Jiang, Y., M. Zhang, W. Wang, and Z. Song, "Reflective and transmissive cross-polarization converter for terahertz wave in a switchable metamaterial," *Physica Scripta*, Vol. 97, No. 1, 015501, 2022.

[19] Shen, Z., Q. Zhang, X. Huang, J. Wu, and H. Yang, "Simultaneous transmissive and reflective polarization conversion cross different operating bands in a single metasurface," *Optics & Laser Technology*, Vol. 169, 110071, 2024.

[20] Yang, H., Y. He, M. S. Tong, L. T. Guo, P. Li, and Y. J. Zhang, "A reflection-transmission multifunctional polarization conversion metasurface," *IEEE Transactions on Antennas and Propagation*, Vol. 72, No. 6, 5099–5109, 2024.

[21] Pramanik, S., S. C. Bakshi, C. Koley, D. Mitra, A. Monti, and F. Bilotti, "Active metasurface-based reconfigurable polarization converter with multiple and simultaneous functionalities," *IEEE Antennas and Wireless Propagation Letters*, Vol. 22, No. 3, 522–526, 2023.

[22] Zhang, C., J. Gao, X. Cao, S.-J. Li, H. Yang, and T. Li, "Multifunction tunable metasurface for entire-space electromagnetic wave manipulation," *IEEE Transactions on Antennas and Propagation*, Vol. 68, No. 4, 3301–3306, 2020.